Supporting information

$(NH_4)_2HPO_4$-mediated closed-pore/pseudographite synergy in thin-walled hard carbon for enhanced Na^+ storage and kinetics

Yatao Chang [a,1], Zhengpeng Yang [a,1], Yufang Cao [b,1,*], Zhao He [c,d], Huili Fu [b], Tongtong Qin [b], Liming Zhao [b,*], Yongyi Zhang [b,c,*]

[a] School of Materials Science and Engineering, Henan Polytechnic University, Jiaozuo 454003, China

[b] Key Laboratory of Multifunctional Nanomaterials and Smart Systems, Suzhou Institute of Nano-Tech and Nano-Bionics, Chinese Academy of Sciences, Suzhou 215123, China

[c] Division of Nanomaterials and Jiangxi Key Lab of Carbonene Materials, Jiangxi Institute of Nanotechnology, Nanchang 330200, China

[d] College of Chemistry and Chemical Engineering, Nanchang University, 999 Xue fu Avenue, Nanchang 330031, China

* Corresponding authors at: Suzhou Institute of Nano-Tech and Nano-Bionics, Chinese Academy of Sciences, Suzhou 215123, PR China.

E-mail addresses: yfcao2019@sinano.ac.cn (Y. Cao), lmzhao2019@sinano.ac.cn (L. Zhao), yyzhang2011@sinano.ac.cn (Y. Zhang).

[1] These authors contributed equally to this work.

Computational Details

All the DFT calculations in our work were performed by the Vienna ab initio simulation package (VASP) [1]. The generalized gradient approximation (GGA) with the Perdew-Burke-Ernzerhof (PBE) functional were used to describe the electronic exchange and correlation effects [2-4]. Uniform G-centered k-points meshes with a resolution of $2\pi*0.04$ $Å^{-1}$ and Methfessel-Paxton electronic smearing were adopted for the integration in the Brillouin zone for geometric optimization. The simulation was run with a cutoff energy of 500 eV throughout the computations. The geometry optimization was considered convergent when the electronic energy and Hellmann-Feynman forces convergence criterion was smaller than 10^{-5} eV and 0.05 eV $Å^{-1}$, respectively. Van der Waals dispersion corrections were treated by the Grimme DFT-D3 method [5-6]. We carried out the potential energy diffusion pathway and minimum diffusion energy barrier of Na on all related graphene systems with the climbing image nudged elastic band (CI-NEB) method, [7] which was implemented in VASP. The method involves optimizing a chain of images which is connecting the initial and final states, and each image of the reaction path can move only in the perpendicular direction.

References

[1] G. Kresse and J. Furthmuller, Comput. Mater. Sci., 1996, 6, 15-50.

[2] J. P. Perdew, K. Burke and M. Ernzerhof, Phys. Rev. Lett., 1996, 77, 3865-3868.

[3] P. E. Blöchl, Matter Mater. Phys., 1994, 50, 17953-17979.

[4] G. Kresse and D. Joubert, Matter Mater. Phys., 1999, 59, 1758.

[5] S. Grimme, J. Comput. Chem. 2006, 27, 1787-1799.

[6] S. Grimme, J. Antony, S. Ehrlich and H. Krieg, J. Chem. Phys. 2010, 132, 15410.

[7] G. Henkelman, B. P. Uberuaga and H. Jonsson, J. Chem. Phys. 2000, 113, 9901.

Supplementary Figures

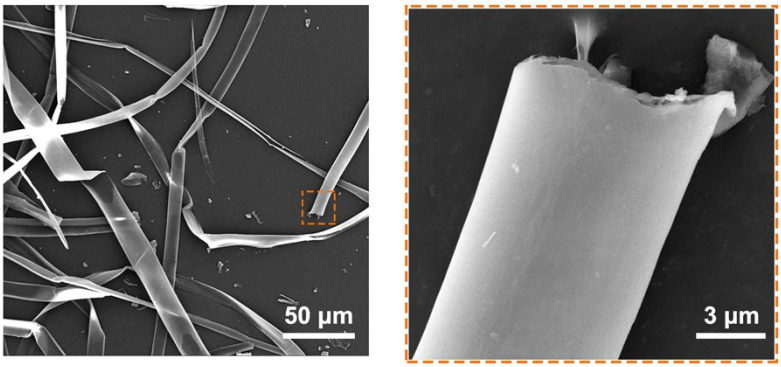

Fig. S1 SEM images of CKF.

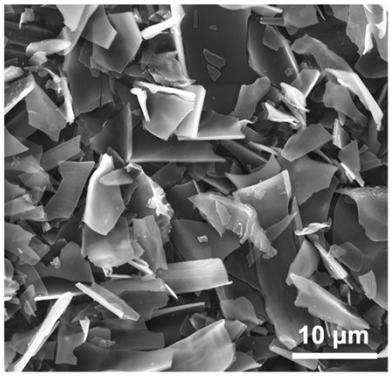

Fig. S2 SEM image of DAP-OKF.

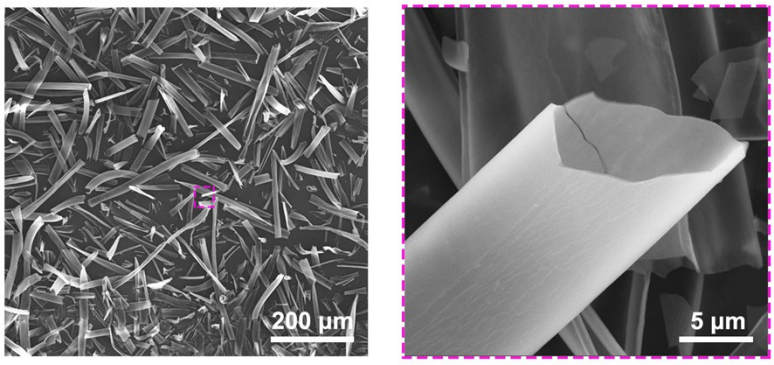

Fig. S3 SEM images of OKF.

Fig. S4 Photographs of CKF, OKF and DAP-OKF.

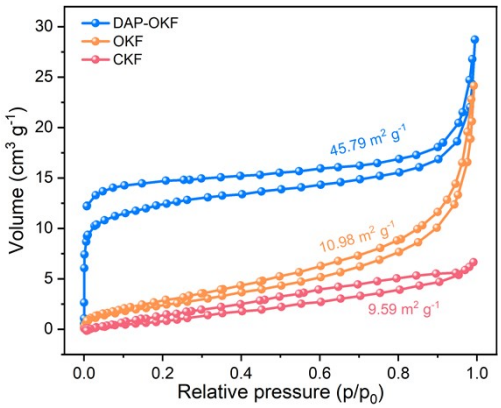

Fig. S5 N_2 adsorption/desorption isotherms of DAP-OKF, OKF and CKF.

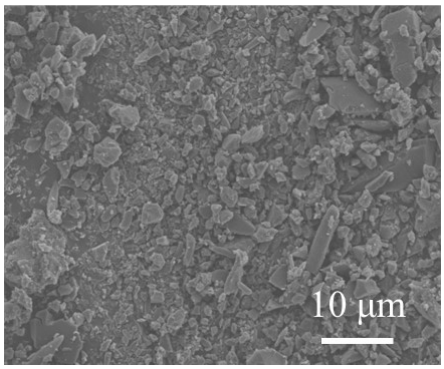

Fig. S6 SEM images of PKF.

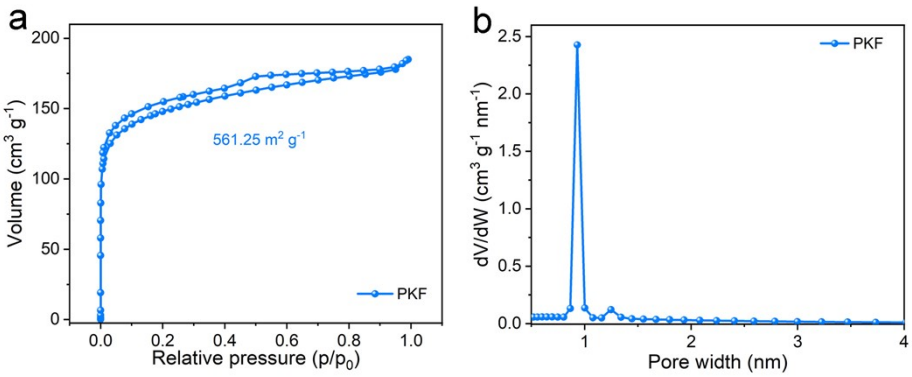

Fig. S7 (a) N_2 adsorption-desorption isothermal curves and (b) pore size distributions of PKF.

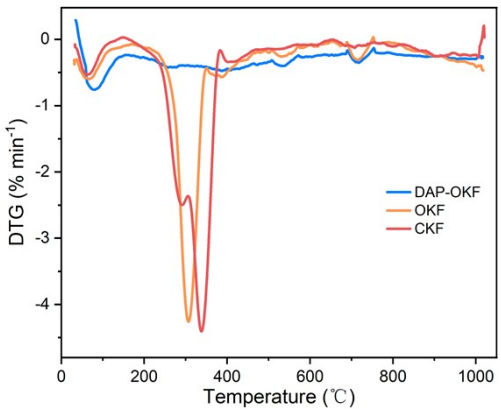

Fig. S8 DTG curves of DAP-OKF, OKF and CKF.

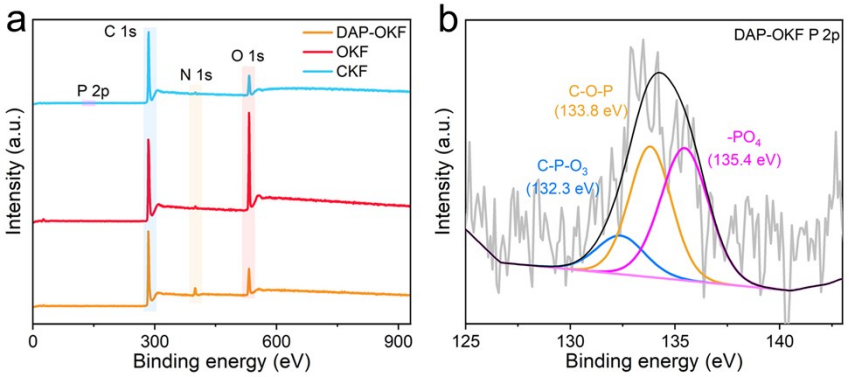

Fig. S9 (a) XPS spectra of DAP-OKF, OKF and CKF. (b) High-resolution P 2p spectrum of DAP-OKF.

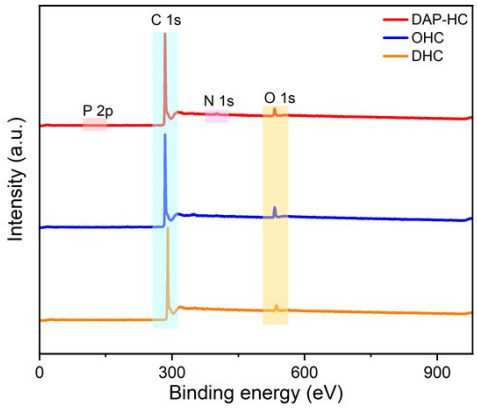

Fig. S10 XPS spectra of DAP-HC, OHC and DHC.

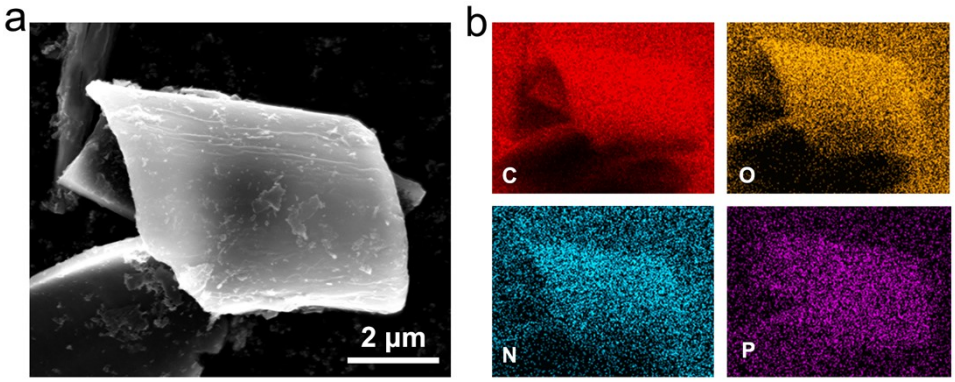

Fig. S11 SEM image of DAP-HC and its EDS element mappings of C, O, N and P.

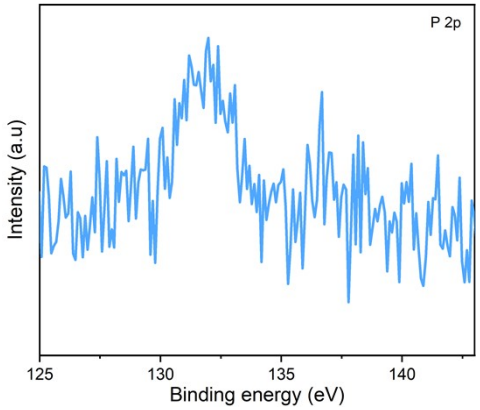

Fig. S12 High-resolution P 2p spectrum (C-P-C) of DAP-HC.

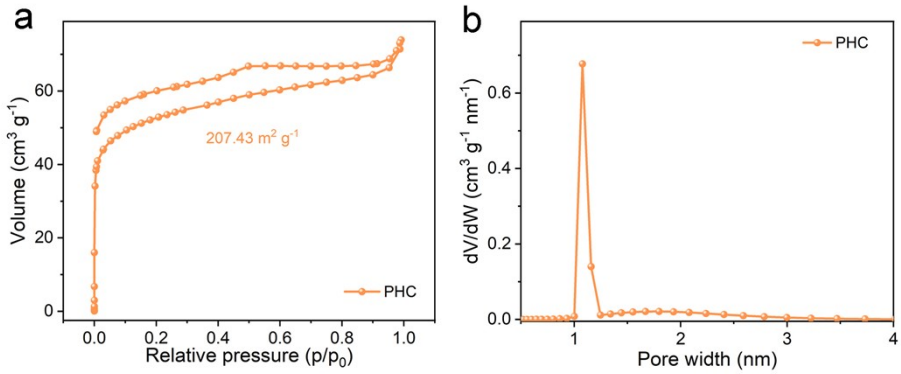

Fig. S13 (a) N_2 adsorption-desorption isothermal curves and (b) pore size distributions of PHC.

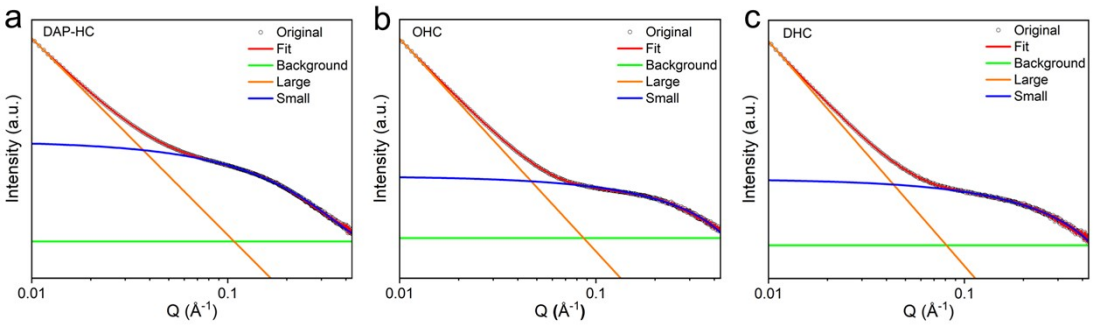

Fig. S14 Fitted SAXS patterns of DAP-HC (a), OHC (b) and DHC (c).

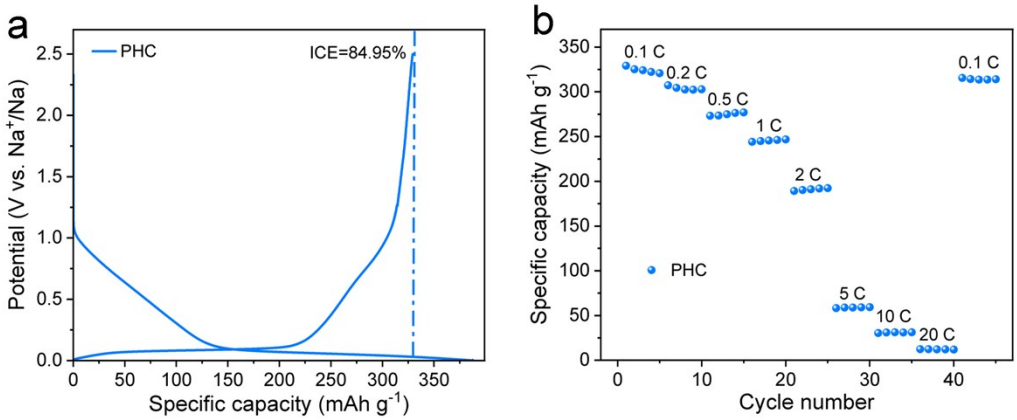

Fig. S15 (a) Initial GCD curves at 0.1 C of PHC. (b) Rate performance at various current rates.

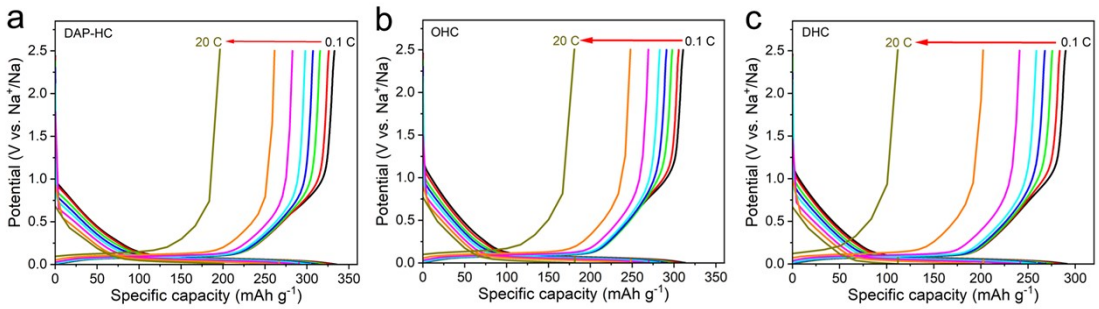

Fig. S16 GCD curves of DAP-HC (a), OHC (b) and DHC (c) anodes at 0.1 C, 0.2 C, 0.5 C, 1 C, 2 C, 5 C, 10 C and 20 C.

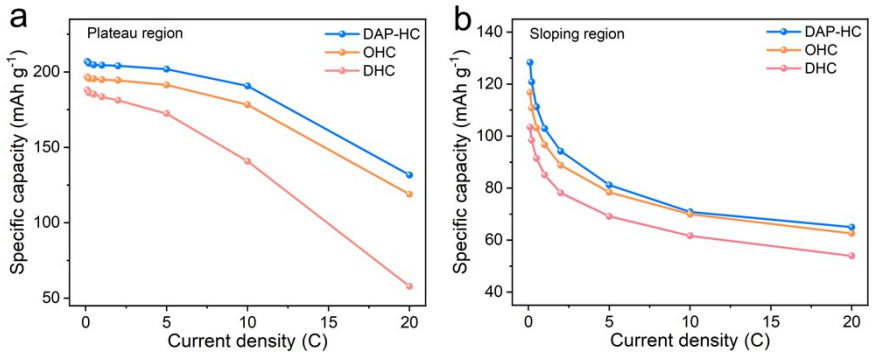

Fig. S17 Plateau (a) and slope (b) capacities of DAP-HC, OHC and DHC at different current densities.

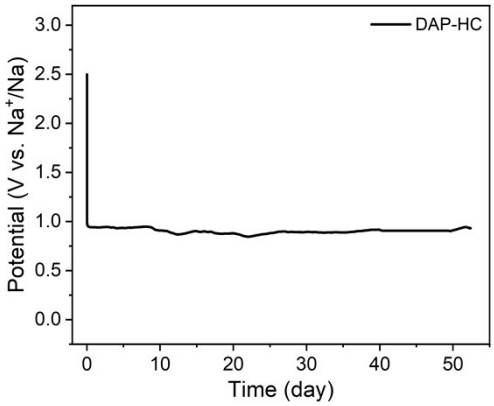

Fig. S18 Self-discharging curves of the open-circuit voltage changes over time for DAP-HC.

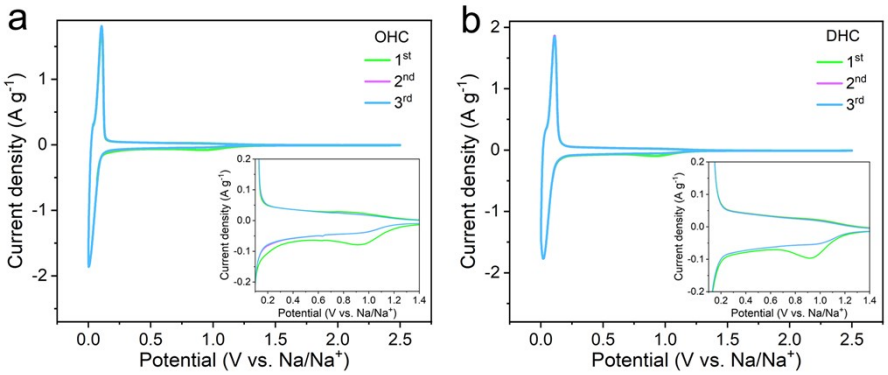

Fig. S19 CV curves of OHC (a) and DHC (b) anodes at 0.2 mV s^{-1}.

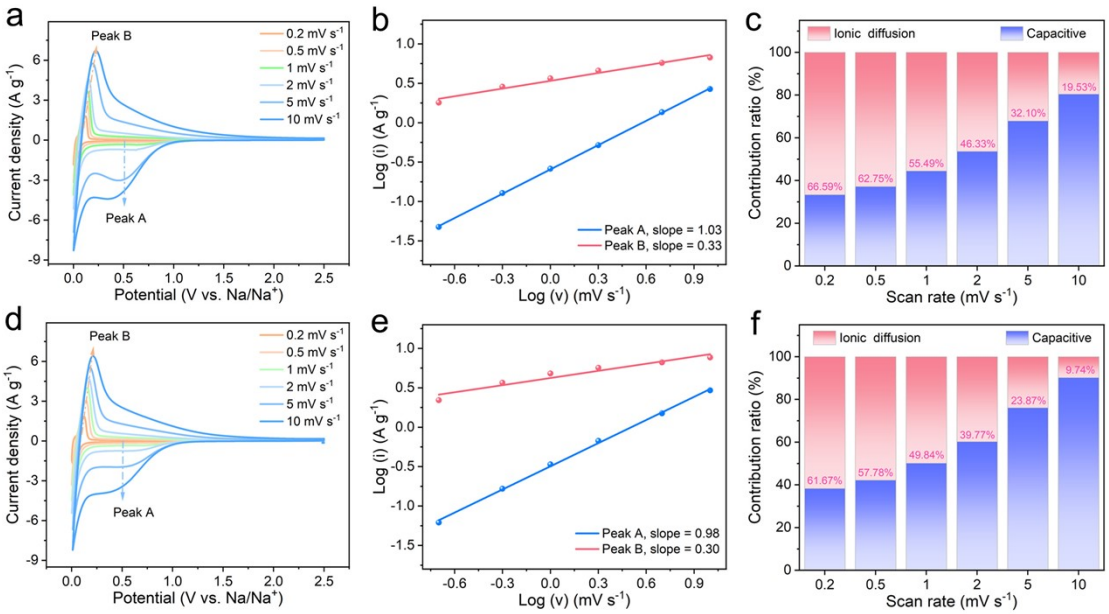

Fig. S20 Kinetic analyses of OHC and DHC anodes for sodium-ion batteries. (a) CV curves of OHC at various scan rates and the corresponding correlations between peak current (i) and scan rate (v) at peak A and peak B (b). (c) Capacitive contribution percentage of OHC at various scan rates. (d) CV curves of DHC at various scan rates and the corresponding correlations between peak current (i) and scan rate (v) at peak A and peak B (e). (f) Capacitive contribution percentage of DHC at various scan rates.

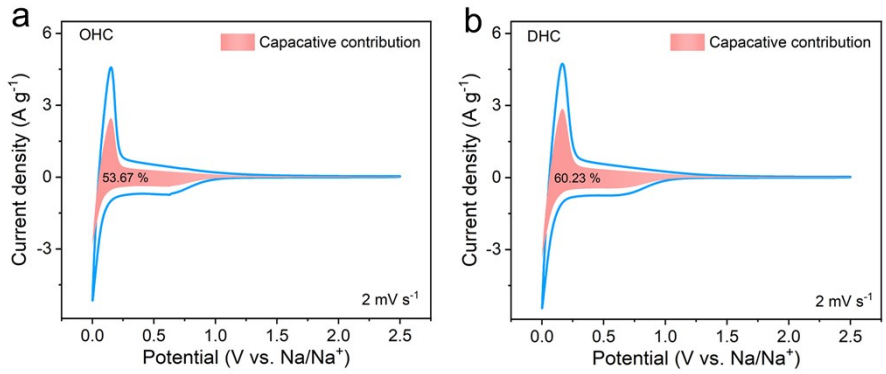

Fig. S21 CV curves of OHC (a) and DHC (b) anodes with a calculated capacitive contribution at 2 mV s^{-1}.

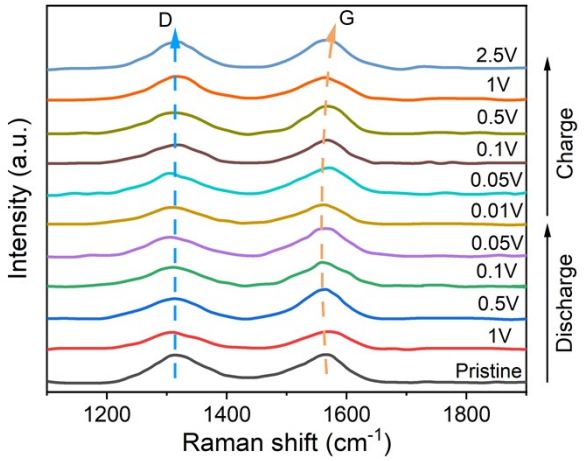

Fig. S22 In-situ Raman spectra of DAP-HC as SIB anodes.

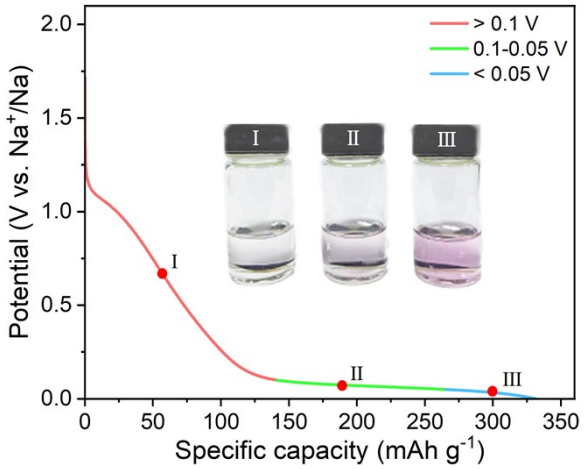

Fig. S23 Optical photographs of electrodes at different discharge stages soaked in an ethanol solution containing phenolphthalein.

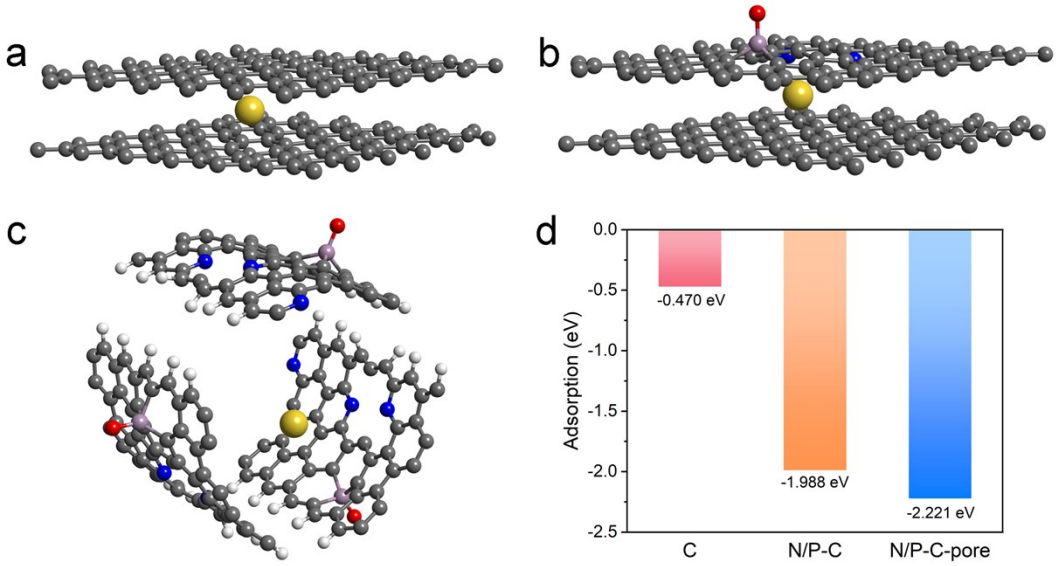

Fig. S24 Optimized configurations of Na adsorbed on different carbon sheets: (a) pristine graphitic layer, (b) N/P co-doped graphitic layer, (c) the closed pore structural model formed by N/P co-doped graphitic layer. (d) Comparison of calculated adsorption energy for Na^+. C: black, N: blue, O: red, H: white, P: purple.

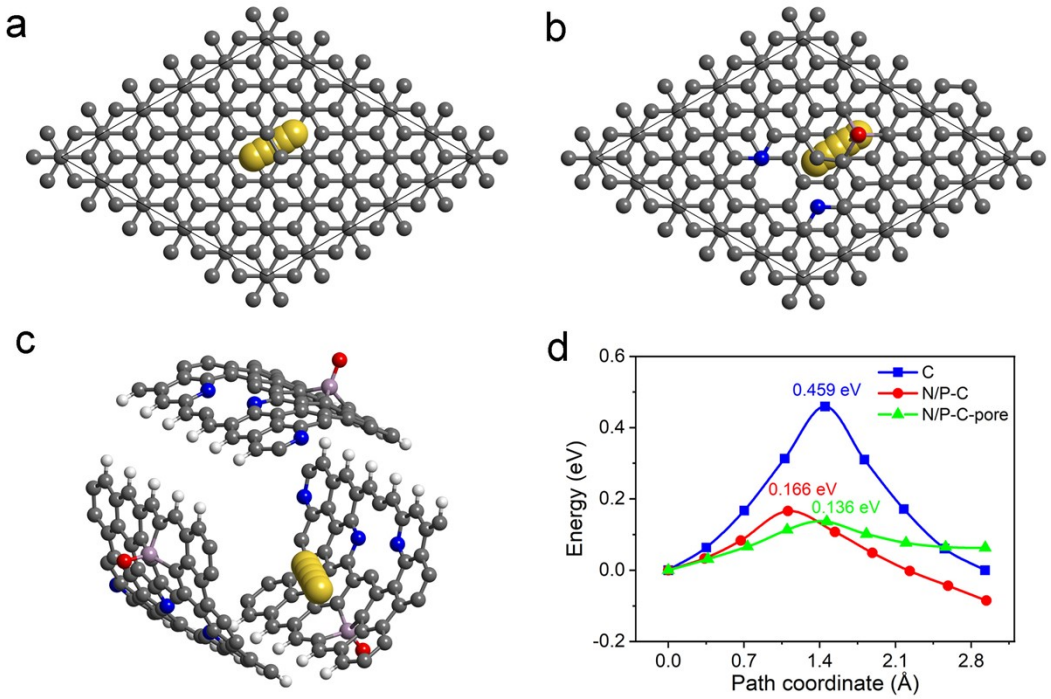

Fig. S25 DFT models for Na^+ diffusion pathways of (a) pristine graphitic layer, (b) N/P co-doped graphitic layer, (c) the closed pore structural model formed by N/P co-doped

graphitic layer. (d) Potential barrier energy for Na^+ at different models. C: black, N: blue, O: red, H: white, P: purple.

Supplementary Tables

Table S1 Structural parameters estimated from N_2 adsorption-desorption results.

Samples	N_2 adsorption	
	S_{BET} (m^2 g^{-1})	V_{pore} (cm^3 g^{-1})
DAP-OKF	45.79	0.3485
OKF	10.98	0.0506
CKF	9.59	0.0109

Table S2 Elemental analysis and XPS analysis-C 1s of DAP-OKF, OKF and CKF.

	Elemental analysis (at.%)				XPS analysis-C 1s (at.%)				
Samples	C	O	N	P	sp^2-C	sp^3-C	C-O/C-N	C=O	O-C=O
DAP-OKF	79.36	13.80	6.41	0.43	21.17	47.15	16.46	9.89	5.33
OKF	72.07	26.55	1.38		17.86	51.20	18.28	7.74	4.92
CKF	85.65	12.06	2.29		15.51	62.36	12.65	6.00	3.48

Table S3 Fitted values from the Porod plot of SAXS data.

	A	B	a	a_1	R (nm)
DAP-HC	$5.62E^{-7}$	$3.58E^{-4}$	4.17	5.94	1.88
OHC	$1.56E^{-7}$	$3.52E^{-4}$	4.36	3.27	1.03
DHC	$7.79E^{-8}$	$3.33E^{-4}$	4.35	3.65	1.15